REPLY TO THE REVIEWER'S COMMENTS

We sincerely appreciate your thorough and thoughtful review. Many of the comments and suggestions required careful consideration and prompted substantial revisions to the manuscript. With your help we have managed to resolve several inconsistencies in the manuscript and clear out many critical points, which hindered readability. We have made every effort to address all remarks. We hope you will recognize the extent of our efforts and find our responses satisfactory.

Thank you very much again for your review.

The Authors

REPLIES TO THE COMMENTS

The reviewer's text is shown black, or replies red and planned changes red-italic. First we address the general comments and then we give replies to specific comments. We are also attaching a Supplement that will be added to a revised manuscript, and also address some of the comments.

Note that proposed changes are still subject to small changes, and not all citations are given!

This is a very interesting paper presenting a modeling approach aimed at showing how the coupling between dissolution, transport in fracture formations, and horizontal head forms a low-karstified rock-blocks which prevent water seepage, up to a threshold of head difference between reservoirs. I very much like the approach, the results, and the layout of the article, and I can see how it will be well suited to HESS. However, three aspects require attention in this study:

General Comment 1: The authors heavily rely on jargon and assume that specific terms and mechanisms are known to the reader. This limits the impact of this study as it targets a narrow readership while overlooking HESS's broad readership. I outlined a few examples and ways to rectify this aspect in the detailed review below.

Reply: We fully agree with your suggestions. We have revised the introduction to better address a broader audience, including readers who are not specialists in karst science. We have emphasized the broader significance of karst aquifers and clarified the relevance of specific terms by replacing them with more familiar language and simpler, more accessible sentences.

The revised introduction (replacing **lines 1-30** in original manuscript) now reads as:

Karst areas occupy approximately 15% of Earth's ice-free land surface. In these regions, the chemical erosion of rock by surface water and groundwater—known as karstification—produces distinctive

surface and subsurface features. Karst aquifers are among the most productive freshwater resources, supplying drinking water to around 20% of the world's population—and more than 50% in some countries (Ford and Williams, 2007). These aquifers are characterized by networks of solution conduits formed within initially fractured and porous rock. The development of these conduits, a process known as speleogenesis, is complex and spans nearly the entire period during which the rock is exposed to groundwater circulation (Dreybrodt, 1996; Yuan et al., 1993).

Karst aquifers can be conceptualized as hierarchically organized conduit systems embedded within a fractured porous matrix. These conduits serve as high-transmissivity flow pathways, channelling water from points of recharge to karst springs. Karstified rocks are also widespread in young orogenic belts, where the high-relief terrain provides favourable elevation differences that facilitate the construction of hydraulic structures such as dams and reservoirs (Milanović, 2000; Yuan et al., 1993; Shen et al., 1997).

However, the construction hydraulic structures in karst areas poses significant engineering challenges. The position, size, and connectivity of existing networks of solution conduits are extremely difficult to predict or detect. As a result, the extent of initial leakage from a reservoir is also hard to estimate (Milanović, 2000, 2018). Furthermore, the high hydraulic gradients induced by such structures can accelerate the formation of new conductive pathways, potentially leading to a rapid increase in leakage—sometimes reaching intolerable levels within the operational lifespan of the structure (Dreybrodt, 1996; Gabrovšek and Dreybrodt, 2001, 2010; Romanov et al., 2003, 2007).

General Comment 2: This work lacks some crucial aspects of the model. This complex model involves multiple processes over extended spatial and temporal scales, yet fundamental elements of this model are absent. What is the grid size and layout, and what is its sensitivity? Was there a convergence test for it? Was the model's sensitivity to key parameters assessed? The authors mention the stability of the solution but provide no data on it. The modeling aspect requires more than just the equations

used and their sequence; a clear section in the paper or an appendix should present these essential components of the model.

Reply: To address this comment, we have added a Supplement (S1, attached to this file), which introduces the fundamental elements of the model. Furthermore, the aspects of this comment (model layout, convergence criteria and stability) are addressed in replies to **specific comments 8, 9, 15 and 16**. We have also checked the equations and their sequence and revised them carefully, as shown in the reply to the **specific comment 12**.

General comment 3: The authors take an engineering approach to the results of their model, which is noteworthy as they draw a specific and tangible conclusion from it. However, the coupling between the transport and reactive mechanisms is a fundamental nucleation phenomenon, where the boundaries lead to an anisotropic, directional change. This phenomenon is observed in other experimental and numerical dissolution processes, where fingers or preferential flows emerge by this coupling (partial list: (Detwiler & Rajaram, 2007; Dijk et al., 2002; Edery et al., 2021; Kang et al., 2003; Molins et al., 2014; Nogues et al., 2013; Rege & Fogler, 1989; Shavelzon & Edery, 2022; Singurindy & Berkowitz, 2003)). Yet this is not referred to in this work, limiting its potential to draw a more general audience and a more general conclusion. These three aspects are echoed in the specific comments below, and I believe that while the last aspect may improve the paper, the first two are essential.

Reply: Thank you for pointing out an issue and providing interesting set of works. We have known some, but not all of them. We have extended the discussion to show this work in the context of nucleation phenomena and added some of the suggested references (see the response and suggested changes in reply to **Specific Comment 23**).

Replies to specific comments

1. The authors make an excellent case supporting their approach in the introduction, yet it will be beneficial to relate each aspect that is either added or missing in previous studies to the figure 1 illustration, thus providing a conceptual picture of the processes at hand.

Reply: We have revised Figure 1 and it caption. This now relates the existence of stagnant cone in the water divide region within porous or fractured media. Lower flow rates in the water divide areas result in less dissolution and lower degree of karstification. The revised Figure 1 is shown below.

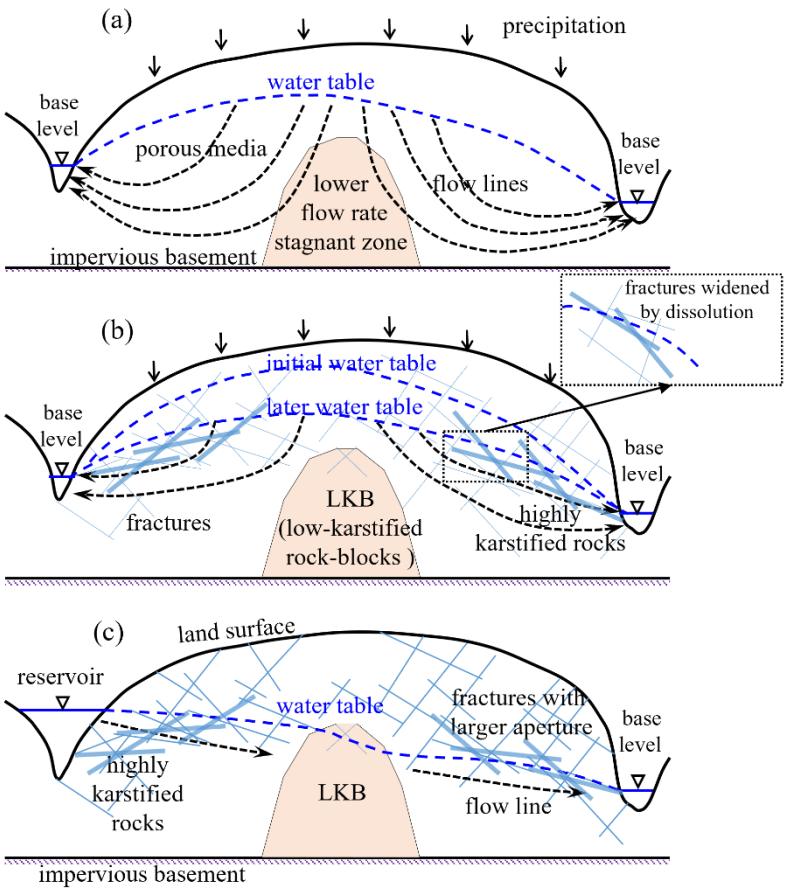

Figure 1: (a) The flow solution reveals the presence of a stagnant zone near the groundwater divide within the porous aquifer. (b) Karstification increases permeability and progressively lowers the water table over time, leading to the formation of blocks that are highly karstified and low karstified blocks (LKB). (c) When reservoirs are constructed, LKB can effectively obstruct leakage across the aquifer.

2. Line 22: “One of the primary issues is the intensification of the natural karstification process due to artificial hydraulic gradients, which can result in persistent and uncontrollable leakage throughout the structure's lifespan”.

   This sentence exemplifies the narrow focus of the paper. In the second sentence of the introduction, we encounter jargon that is not properly explained. We have no idea what the artificial part is in these hydraulic gradients and why it leads to “persistent and uncontrollable leakage.” I suspect that not all potential readers remember exactly what the “karstification process” is. HESS aims at a broad readership; therefore, an effort should be made to address this broad readership by thoroughly explaining the terms and concepts.

   Reply: We have addressed the issues raised in the comment in the new Introduction (Page 3).

3. Introducing Figure 1 earlier and including additional features, such as the permeability linked to fracture aperture changes and the chemical gradients that shape the LKB zone, can help rectify this. The latter will significantly aid in clarifying the cause-and-effect relationship that the authors seek to establish in their work. This approach will give readers a conceptual framework from the outset and elucidate the terms and concepts of the study.

   Reply: Figure 1 has been updated. See the reply to Comment 1 (Page 5).

4. Line 69: Explain what epikarst is.

Reply: Epikarst is the uppermost layer of vadose zone, an interface between the surface unconsolidated material and karstified carbonate rocks. Epikarst is capable of delaying, storing and locally rerouting vertical infiltration to the deeper zones of underlying karst aquifer. We have explained this specific term at its first appearance in the revised manuscript.

However, since the specific role of epikarst is not considered in this work, we have revised the paragraph (lines 70 to 75 of original manuscript), which now reads:

As demonstrated by the models of Gabrovšek and Dreybrodt (2001) and Kaufmann (2003), the evolution of unconfined karst aquifers is most pronounced near the water table. In brief, these models do not explicitly account for the details of flow and dissolution in the vadose zone—the region between the surface and the water table—but instead assume gravitational flow that reaches a specific level of chemical saturation with respect to calcite. Nevertheless, within the phreatic zone, water is typically least saturated with respect to calcite near the water table, and thus possesses the highest potential for dissolution (often referred as aggressivity) in this region. The numerical methods employed in these studies primarily concentrate on the evolution of relatively homogeneous fracture networks, rather than the random fractures found in natural karst aquifers.

5. Line 71: Not sure "aggressive" is clear in this context.

Reply: See the change of the paragraph given above. Aggressive means that "the solution is capable of dissolving carbonates". We avoided the use of this term and used: *water is typically least saturated with respect to calcite near the water table, and thus possesses the highest potential for dissolution.*

6. Line 87: Explain what "speleogenesis" is.

Reply: We have introduced the term in the revised Introduction (see reply to General comment 1)m where we state: *The development of these conduits,* ***a process known as speleogenesis****, is complex and spans nearly the entire period during which the rock is exposed to groundwater circulation.*

7. Line 95: add a space after "(4)"

Reply: Done.

8. While the criteria for transitioning between equations 1 and 2 are clear, the actual continuous transition between equations 1 and 2 or vice versa is not clear. How do we continuously transition from the laminar to the turbulent approximation without discontinuities in the flux? The flux mass balance presented in Eq. 4 should also be addressed in this context.

   Addendum: at the end of the paper, we learn that equation 2 was not used throughout the simulations (or so I understood from the following sentence: "Turbulent flow did not occur throughout the simulations initiated with natural, original fractures."). If that is the case, why present it?

Reply: The model allows turbulent flow, however as noticed by the reviewer, in the presented simulations turbulence never occurred. Transition from laminar to turbulent flow and vice versa is a complex phenomenon. Most models calculate friction factors from the Reynolds number, which is also criterion for onset of turbulence. Different approaches of how to deal with noncontinuous phenomena are being used, modellers often invoke some type of hysteresis, and another elegant approach is use of Churchill equation, which gives a smooth continuous friction factor as a function of Reynolds number in the transition zone. How precise we want to model, depends on what we want to model and how important the proper treatment of laminar/turbulent transition is. Experiences from previous modelling of karst networks evolution showed that different

algorithms gave practically same results. Therefore, here we use a rather crude approach, where we simply take the flow with higher frictional losses. In fact this means that we neglect transition zone and switch directly from laminar to fully turbulent flow. Figure R1 shows flow through a fracture as a function of hydraulic gradient calculated for laminar flow and from Lomize approximation. For Re<2020 Eq.1 is used and Eq.2 is used for Re>2020.

We have added a text at the end of section 2.1 (before the Line 110 in the original text):

The transition from the laminar to the turbulent flow regime is here introduced at the point where turbulent frictional losses exceed those associated with laminar flow. The factor in Lomize equation (Eq. 3), is set so that transition occurs at a Reynolds number of 2020. This simplification omits the transitional flow zone, resulting in a smooth increase in flow rates as turbulence sets in. However, in the results presented, the flow remains within the laminar regime throughout the simulations.

(a) Transition from cubic law to Lomize equation

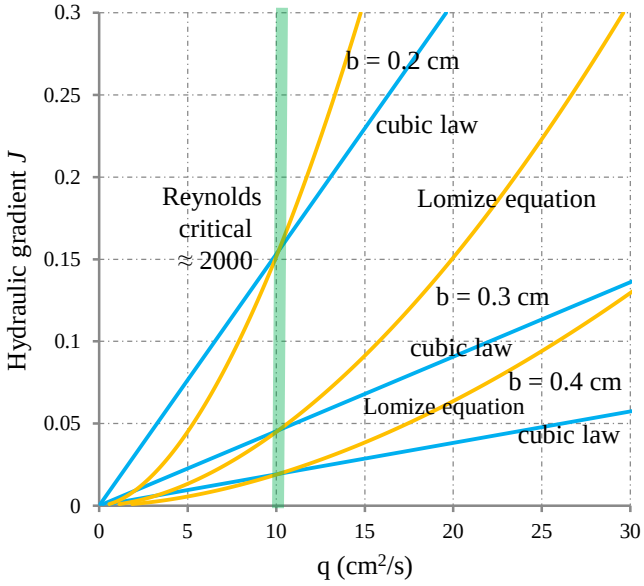

(b) Transition from Darcy's law to Darcy-Weisbah (cited from MODFLOW-CFP manual)

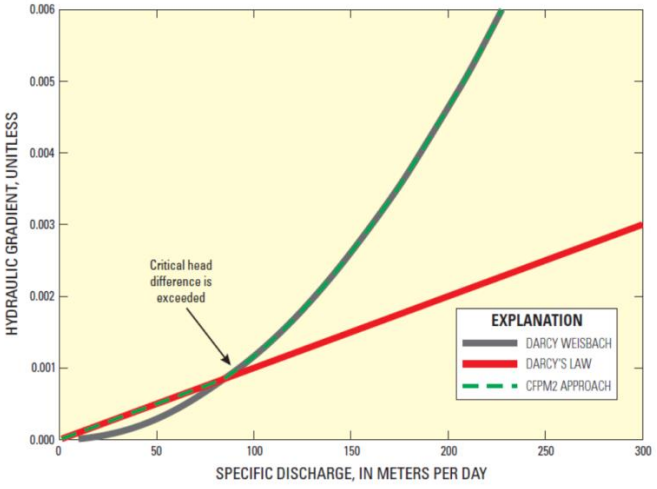

Figure R1. The approximation of transition between laminar and turbulent flow.

9. Line 121: Is Figure 2 an illustration, actual layout, or sub-layout of the fractured domain? Also, the dimensions are critical in understanding the model framework (Reynolds number, head differences, etc.). Referring to boundary, seepage, and head without their dimensions seems inadequate.

Reply: Figure 3 (renumbered) presents just the concept of how the position of WT is calculated. We have extended the caption to make it more readable. Furthermore, since both reviewers found it disturbing, we have dropped the somehow misleading terminology of inner, middle, and outer iteration and changed it to **Confined Flow Calculation, node-by-node iteration, layer-by-layer iteration. The notation is changed throughout the test.**

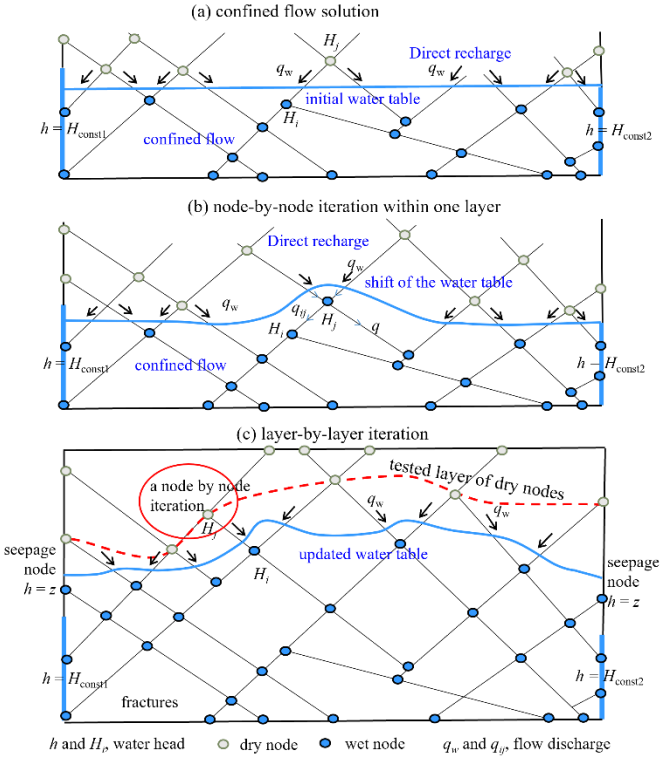

Figure 3.(renumbered) *Conceptual presentation of flow calculation in the fracture network. (a) Boundary conditions for Confined flow calculation performed at* ***every*** *iterative step. (b) Node-by-node iteration: testing wetting of a dry node across a layer. (c) Layer-by-layer iteration.* H_i *and* H_j *are heads at wetted nodes,* q_w *is direct recharge from the vadose flow, z is elevation of the node.*

10. Section 2.2.2: Please refer to Figure 2 when explaining the necessary steps in finding the water table.

Reply: Thank you for pointing to insufficient referencing to Figure 2. In the revised manuscript we have updated the text to fit the figure.

Introductory paragraph (Line 115) of Section 2.2 now outlines the search for the water table; it now reads:

Each evolution time step requires the calculation of flow, dissolution, solute transport, and the corresponding changes in fracture aperture. Accurate flow calculation depends on determining the position of the water table at each time step. This is achieved through an iterative process, in which the water table position is updated until specific convergence criteria are met, as described in Section 2.2.2. The procedure is illustrated in Figure 2. At each iteration, the current approximation of the water table defines a set of boundary conditions (Figure 2a): prescribed recharge at water table nodes, seepage conditions (where hydraulic head equals surface elevation) at seepage nodes, and either no-flow or constant-head conditions elsewhere. The flow solver (Confined flow solution) is then invoked to compute flow rates and hydraulic heads at all nodes. Water table nodes are subsequently searched node by node within each layer (Figure 2b, node-by-node iteration) and layer-by-layer throughout the domain (Figure 2c, layer-by-layer iteration).

We also intend to add a flow chart (Figure R2), which will summarise the steps described in section 2.2.2.

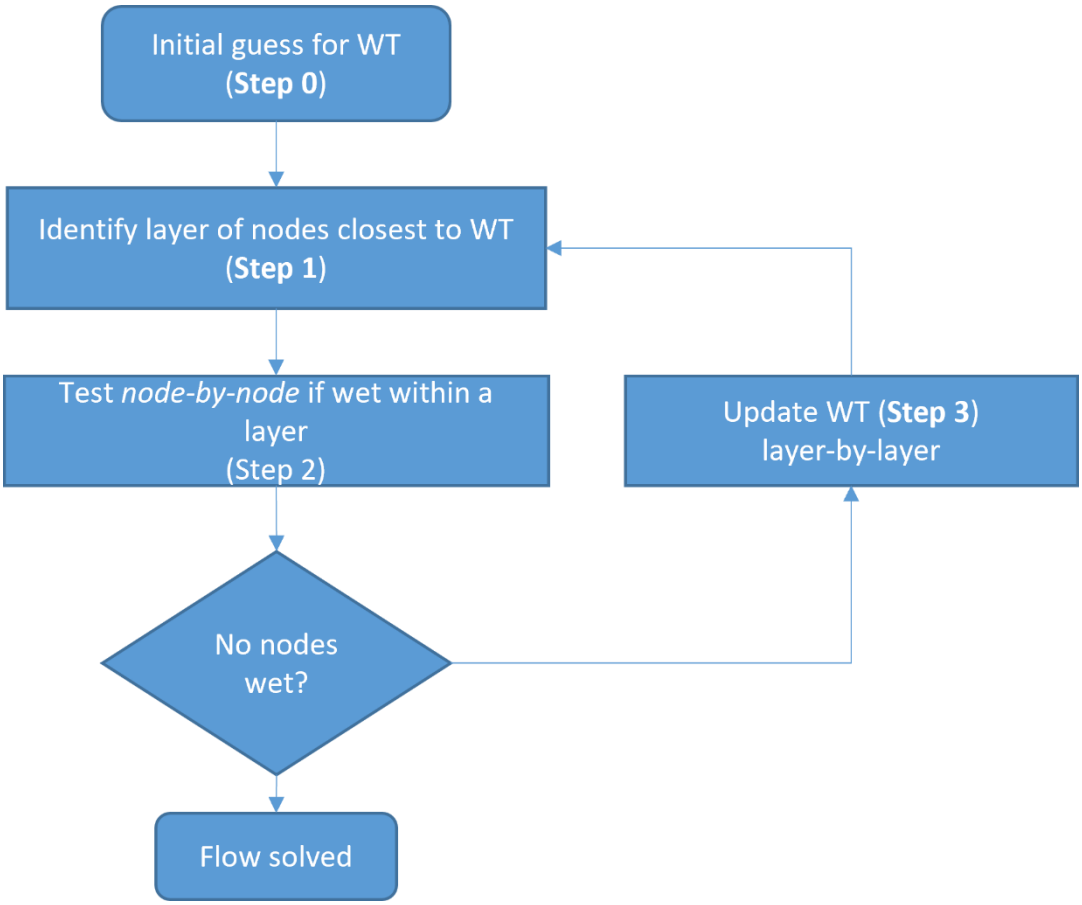

Figure R2: Flowchart of the flow solution.

11. Section 2.3: The "H_2O-CO_2-$CaCO_3$" system is heavily influenced by pH. Although the CO_2 concentration can provide an approximation, this is only valid within a limited range of pH values. Please address this aspect.

Reply: In most carbonate karst areas, the CO_2 is considered as a primary source for the dissolution potential of natural water with respect to carbonates. The pH is of course a master variable of the system and is as such used to calculate equilibrium. In a pure CO_2-water-calcite system, the protons are primarily delivered from the hydration of CO_2 molecules, and consumed by the

formation of bicarbonate. Therefore, the availability of CO_2 in this system, determines the solubility, or equilibrium concentration. The undersaturation defines the rate of dissolution according to the experimentally derived rate laws (Eq. 7 and 8).

We have revised paragraph (from line 158) to better clarify these concepts. It now reads:

where k_1 and k_n are rate constants (in mol·cm^{-2}·s^{-1}), C represents the concentration of Ca^{2+} ions (in mol·L^{-1}), and C_{eq} denotes the equilibrium concentration of the H_2O-CO_2-$CaCO_3$ system. The C_{eq} can be calculated from the concentration of calcium and dissolved CO_2 of the solution at the water table. This equilibrium state results from complex flow and dissolution processes occurring in the vadose zone, which are beyond the scope of this study. We take uniform equilibrium concentration (2 mmol/L) and uniform saturation ratio (C_{in}=0.92C_{eq}) at water table nodes. The reaction follows a linear rate law up to the switch concentration C_s, transitioning to a nonlinear rate law between C_s and C_{eq}. Here we assume that rates are entirely controlled by surface reaction, and ignore the concentration gradient perpendicular to flow. This approximation is valid for situations where the solutions are close to equilibrium, which is mostly the case in the presented scenarios. The reaction order n and the switch concentration….

12. Furthermore, a convective approach for the laminar case must approximate the reactant depletion as it reaches the fracture surface by some rate law. Since eq. 9-11 do not consider the fracture thickness b_{ij} while the illustration in figure 3 does, I am a bit confused about this matter. Please provide clarity on this aspect.

Reply: We agree that this can be told better. The aperture controls the flow rates, which in turn control the increase of calcium concentration along the fracture. Furthermore, the dissolution rate depends on the surface reaction, determined by concentration of species at the solution-mineral interface, and diffusion transport, which is controlled by concentration gradients within

the fracture. Diffusion rates, among others depend on aperture width, which is not considered in the model. We here approximate the dissolution rates by experimentally determined surface reaction rates as given in Eq. 7 and 8. Taking the fact that the inflowing solution is close to equilibrium, the approximation of surface controlled reaction is reasonable.

We have clarified this in the text. Furthermore, we have moved the calculation of change of concentration within a fracture and corresponding mass and aperture change to appendix.

The paragraph (Lines 166-185) will be replaced by:

The change in concentration along an individual fracture can be determined by applying the principle of mass conservation within a water parcel passing along the fracture. This can be easily analytically calculated for parallel plan (the flow perimeter P(x) is constant) fracture, as shown in the supplements. Change of concentration along the fracture can be converted to mass removed from the fracture walls and the change of aperture during time Δt,

$$\Delta b = \frac{\Delta C \; q \; M_{CaCO_3}}{\rho \; L} \Delta t \qquad (9)$$

where L is the fracture length, ρ is the density of calcite (2.5 g/cm^3) and M_{CaCO_3} is the molar mass of calcite (100 g/mol), and q the linear flow density.

13. Line 182: Is the mass removal term converted to a volume change from which the b_{ij} is updated? If so, what is the conversion constant from moles to volume?

Reply: This is now described in the paragraph above.

14. Line 204: Correct grammar in “These analyses”

Reply: Done.

15. Figure 4: While we agree on the analytical solution deviation, the magnitude of the deviation between the numerical value and the analytical solution is around 50%, which necessitates further elaboration on why it is so large.

Reply: We fully agree that the analytical solution presented is not sufficient for the flow validation. Actually the analytical solution is based on Dupuit approximation, which neglects vertical flow and seepage face. We have now used MODFLOW and its DRAIN module to test the validity of our solution on basic cases and moved the test results to Supplements.

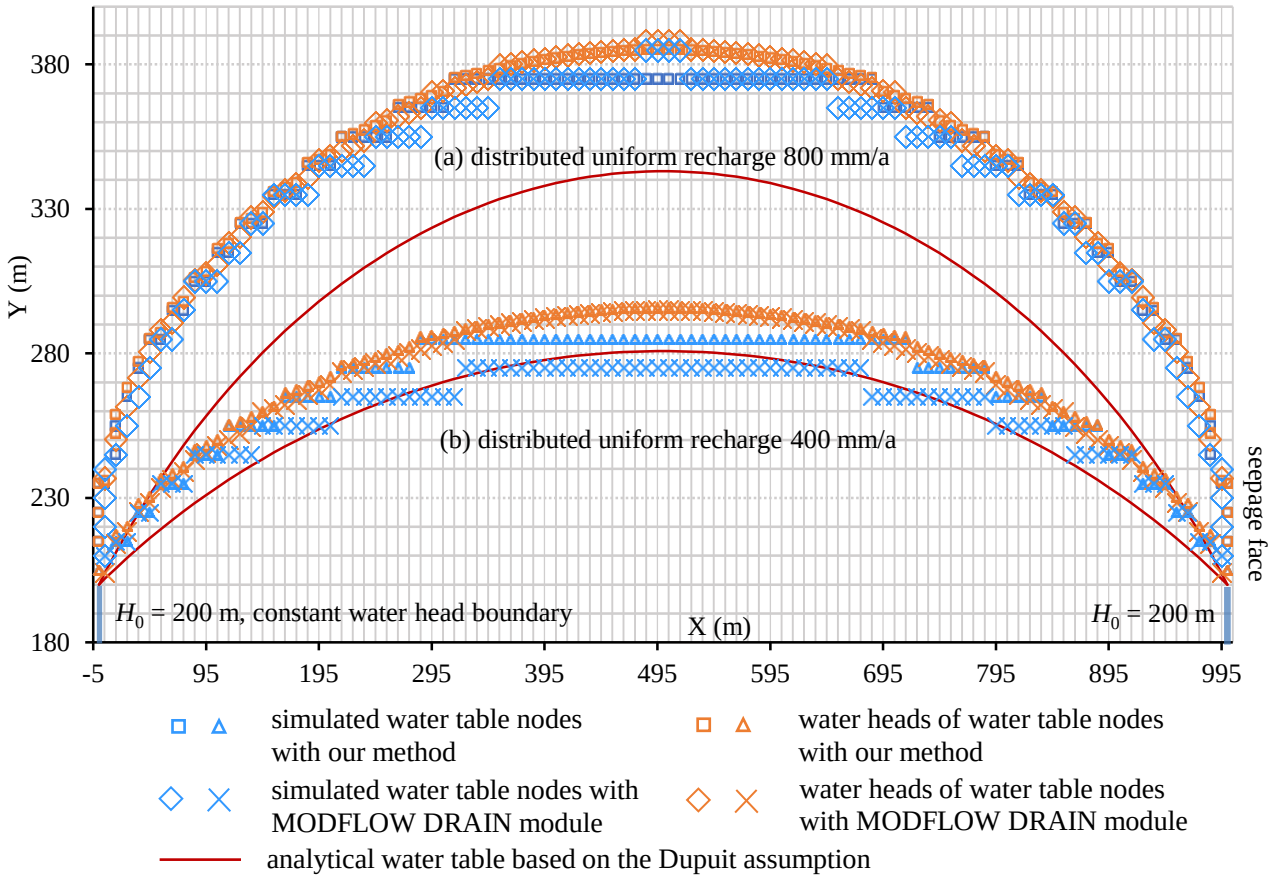

Figure S2.1. Water tables and corresponding heads validation with MODFLOW and Dupuit analytical models for two distributed uniform recharge conditions.

16. Section 2.4.2: It's hard to understand how well the model performs since we do not have any specific case to compare it to, aside from the analytical solution, which we established as inadequate. How can we be sure that the model works as it should? In terms of numerical analysis, there is no mention of grid size sensitivity, convergence, or stability of the numerical code, which are standard practices. The authors should present these aspects of the code so that we can appreciate it accordingly.

Reply: As written above, the position of the water table estimation is in a good agreement with with MODFLOW calculation for porous media with equivalent hydraulic conductivity. The accuracy of confined flow solution is assured by flow balance and head tolerance (H_{tol} = 10^{-4} m and Q_{tol} = 0.1 cm^2/s). The flow solver uses preconditioned conjugate gradient approach for sparse matrix.

Although we deal with *irregular grid*, the accuracy also somehow depends on the fracture length. Namely, the head at the water table nodes is between the elevation of the WT node and the elevation of the nearest dry neighbour node. The widening of the fracture connecting these nodes is not considered. This inconsistency is smaller for small grids.

17. Line 218: "on the both sides" should be "on both sides"

Reply: Done.

18. Line 219: "…the algorithm performed well in modelling the water table in heterogeneous network." Well, compared to what? These statements appear throughout the paper, yet they are not supported by any comparison or measurement that helps us understand what "well" means. The only reference is to the ill-fitted analytical solution.

Reply: We hope that we have adequately responded to the comment in answers given above.

19. Table 1: What are the dimensions of the directional term? Angle?

Reply: Yes, this refers to the angle between the fracture and the horizontal, expressed in degrees. We have corrected the directional reference of the angle in the revised manuscript.

20. Additionally, the mean length of the fractures is quite large. Is this realistic? Why was this length chosen? It appears that ten well-connected fractures may dominate the simulation

Reply: The choice of parameters for stochastic fracture generation is rather arbitrary, but fracture lengths span quite a large interval which corresponds to possible natural settings. The realisation used here is just one of the possible ones, used to test the concept of LKB. Further modelling would be needed to show the extent and hydraulic contrast of LKB in various setting, which remains a further perspective.

21. Line 252: Please clarify the term "evolution time step."

Reply: We have corrected "evolution time step" to "time step" in the revised manuscript. The system goes through a set of stationary states, when flow dissolution and widening is calculated. The time spent in the state is called a time step. The choice of time step is heuristic, and is a compromise between the accuracy and computational demand. We have compared the result of simulation for different time steps and the differences become negligible, when time steps are smaller than the one taken in this work.

22. Line 255, figure 8 caption: What does "ka" stand for? I'm assuming it refers to time, but no dimensions have been provided. This should be clarified in Figure 8, not Figure 10. Additionally, the heat map for the aperture could be confused with the head heat map. It is unclear whether it is necessary.

Reply: The "ka" stands for one thousand year. We have corrected it with an explanation in Figure 8. To avoid confusion, we have also rotated the heat map of aperture Figure 9 to be

vertical in the revised manuscript. Figure 8 and Figure 9 have been renumbered to Figure 6 and Figure 7. Figure 7 is shown below:

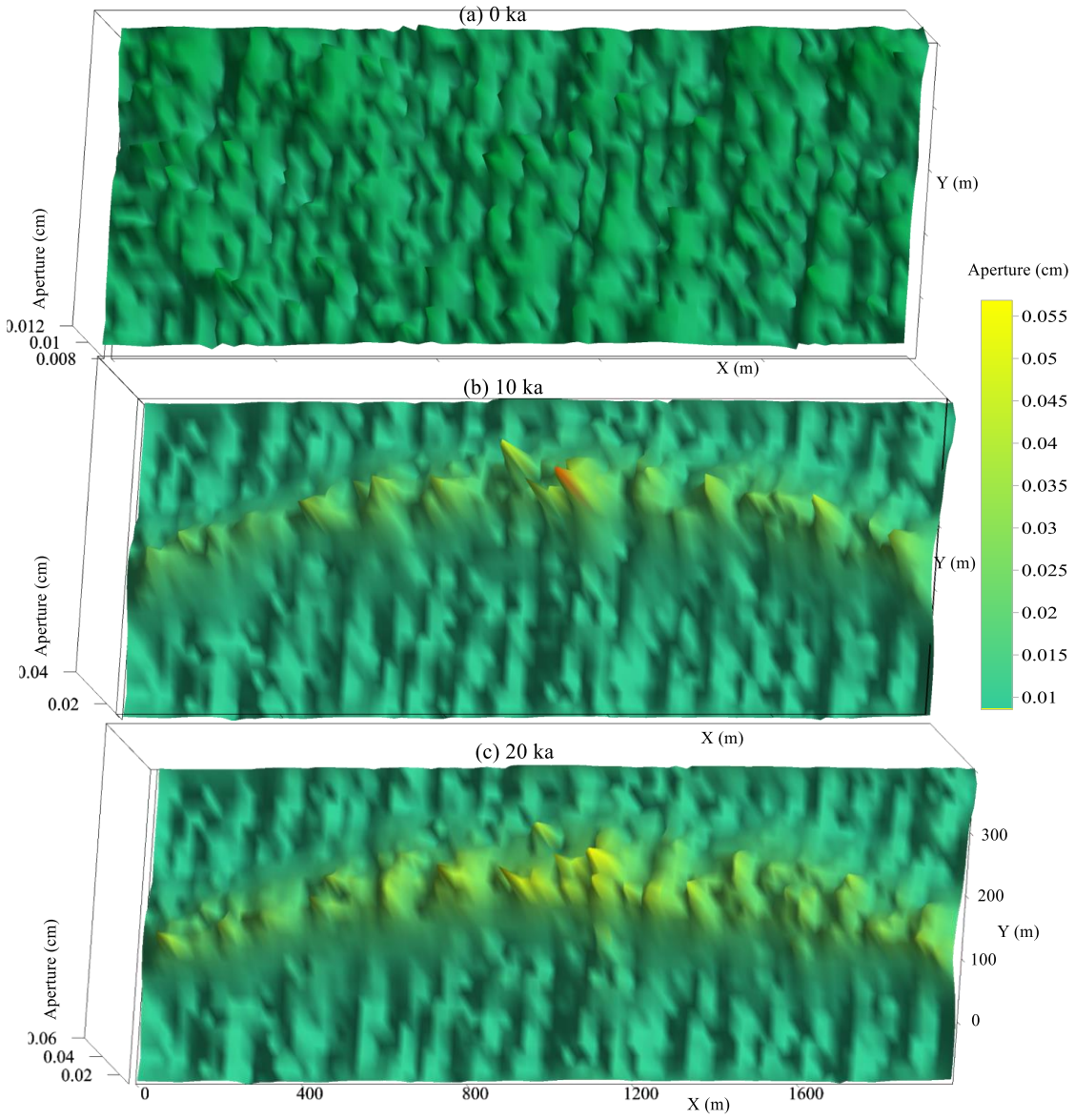

Figure 7(renumbered) Evolution of fracture aperture at 0 ka (a), 10 ka (b) and 20 ka (c) under natural conditions.

23. Section 3.3: In this section, the authors relate the change in aperture to the location of the aquifer, as evident in Figure 11, and also relate the change in flux in a similar manner. However, the cause and effect suggest that the higher potential near the boundaries dictates higher fluxes, and as the flux increases, so does the reaction rate, which widens the aperture. This is a nucleation phenomenon observed in many studies on dissolution, specifically in the context of permeable structures.

Reply: We agree that the text in section 3.3 needs some revision to more clearly address the feedback mechanisms between flow and dissolution rates.

We have added the paragraph at the end of Section, which discusses the issues raised in the comment:

Karstification represents a form of nucleation, where flow-induced dissolution and changes in porosity are coupled through feedback mechanisms (Eder et al., 2021; Molins et al., 2014) . *In unconfined aquifers under constant recharge conditions, dissolution is most intense near the water table. This process creates a highly permeable fringe that effectively channels inflow toward both sides of the water divide. As this fringe migrates downward across the aquifer cross-section, it leaves behind a distinctive porosity imprint. Simultaneously, it inhibits deeper penetration of the inflowing solution, favoring the preferential development of horizontal fractures. Moreover, flow along the water table increases progressively from the water divide toward the discharge points. As a result the water divide zone is less karstified than the regions close to the output. Similar anisotropic, directional changes, including fingers or preferential flows, has also been observed through experimental studies and other numerical simulations (Shavelzon and Edery, 2022; Singurindy and Berkowitz, 2003).*

24. Line 295: I find the K calculation very interesting. To begin with, the fact that there is only dissolution in this setup means that the LKB is a "residual" permeability, indicating that while some permeabilities have increased, the LKB remained unchanged. However, the K is calculated directly for a subsection, and figure 12, as well as a close examination of figure 8, shows that there is an anisotropic change in the aperture, where horizontal fractures experience more dissolution than the vertical fractures. This also leads to the formation of the LKB and the observed changes in flux. However, this structural anisotropy is not discussed or quantified in this context, although it is clear that the horizontal head difference drives the anisotropy. This emergence of anisotropy can be found in many studies on rock dissolution, where preferential flows arise due to these boundary conditions coupled with reactive transport. As this emergent behaviour appears in similar fields, the connection should be made among them.

Reply: We have included discussion in a previous comment.

Reference list:

Detwiler, L. R., and Rajaram, H.: Predicting dissolution patterns in variable aperture fractures: Evaluation of an enhanced depth-averaged computational model, Water Resour. Res., 43, W04403, https://doi.org/10.1029/2006WR005147, 2007.

Dijk, P. E., Berkowitz, B., and Yechieli, Y.: Measurement and analysis of dissolution patterns in rock fractures, Water Resour. Res., 38, https://doi.org/10.1029/2001WR000246, 2002.

Edery, Y., Stolar, M., Porta, G., and Guadagnini, A.: Feedback mechanisms between precipitation and dissolution reactions across randomly heterogeneous conductivity fields, Hydrol. Earth Syst. Sci., 25, 5905–5915, https://doi.org/10.5194/hess-25-5905-2021, 2021.

Kang, Q., Zhang, D., and Chen, S.: Simulation of dissolution and precipitation in porous media, J. Geophys. Res., 108, https://doi.org/10.1029/2003JB002504, 2003.

Molins, S., Trebotich, D., Yang, L., Ajo-Franklin, J. B., Ligocki, T. J., Shen, C., and Steefel, C. I.: Pore-scale controls on calcite dissolution rates from flow-through laboratory and numerical experiments, Environ. Sci. Technol., 48, 7453–7460, https://doi.org/10.1021/es5013438, 2014.

Nogues, J. P., Fitts, J. P., Celia, M. A., and Peters, C. A.: Permeability evolution due to dissolution and precipitation of carbonates using reactive transport modeling in pore networks, Water Resour. Res., 49, 6006–6021, https://doi.org/10.1002/wrcr.20486, 2013.

Rege, S. D., and Fogler, H. S.: Competition among flow, dissolution, and precipitation in porous media, AIChE J., 35, 1177 – 1185, https://doi.org/10.1002/aic.690350713, 1989.

Shavelzon, E., and Edery, Y.: Modeling of Reactive Transport in Porous Rock: Influence of Peclet Number, EGU22-8059, https://doi.org/10.5194/egusphere-egu22-8059, 2022.

Singurindy, O., and Berkowitz, B.: Evolution of hydraulic conductivity by precipitation and dissolution in carbonate rock, Water Resour. Res., 39, W1016, https://doi.org/10.1029/2001WR001055, 2003.

Reply: Thank you for your suggestion. We have reviewed the recommended papers and found that they offer valuable new perspectives on our work. While we have not yet had the opportunity to study them all in depth, we have cited several in the revised manuscript (see above). We intend to incorporate these insights more fully into our future research.

Supplements

S1 Model details & validation

At each time step, the convergence status is recorded in the runtime output file. An example is available on our GitHub repository at Fracturetokarst2024/slurm-17392021.out.. This file includes key indicators such as the number of iterations required for solving the iterative flow equations for confined flow solver, water head errors, and total flux balance. Iterations are controlled internally both node-by-node and layer-by-layer. If the confined flow solver encounters convergence issues, the model reverts to the last successful state and proceeds by testing an the next dry node. To assess the model's accuracy, results were benchmarked against MODFLOW simulations, as described in the subsequent section.

We also explored the model's behavior under different flow regimes by simulating the coexistence of turbulent and laminar flows. These tests confirmed the numerical stability of the model. Additionally, the model is capable of generating random fractures, which are used directly in flow and dissolution computations. These fractures vary in shape and size and are not constrained by the underlying computational grid.

A high-performance computing environment is essential for achieving long-term stability in water table simulations. The calculations were performed on a platform using a Chinese Hygon C86 7185 32-core processor, running CentOS Linux 7. For these simulations, we utilized 8 cores on a single compute node.

S 2 Test of the water table in a homogeneous fractured aquifer

To verify the numerical model, we first compare the results for the homogeneous network with MODFLOW (Harbaugh et al., 2000) and the analytical solution derived using the Dupuit assumption, which can be expressed as follows:

$$H=\sqrt{H_0^2-\frac{w}{K_x}X^2+\frac{wS}{K_x}X} \tag{S1}$$

where H_0 is the river base level, K_x is the equivalent horizontal conductivity in m/d, S is the aquifer length, X is the distance from the left river boundary, and w is the intensity of rainfall recharge.

The homogeneous fracture network is shown in Figure S2.1. We assume translational symmetry and therefore use 2D domain populated by fracture. The horizontal dimension of the domain is 1000 m and vertical 400 m. The distance between the fractures in both the X direction and the Y direction is 10 m. The aperture is 0.01 cm for all the fractures. Along the two side boundaries, nodes lower than 200 m in height are given a constant water head of 200 m. Nodes above 200 m have seepage boundary conditions. The two recharge conditions were tested at 400 mm/a and 800 mm/a.

Within the MODFLOW validation, we calculate the equivalent horizontal K_x and vertical K_y by treating the aquifer as having confined water head boundaries in the X and Y directions, respectively. The conductivities are proportional to the ratio between the resulting flux and the head difference. The horizontal and vertical K values are virtually identical, both approximately 0.00705 m/d. The DRAIN module in MODFLOW was used to model the seepage face by setting each boundary node above the constant head with drainage function, which worked as its water head became higher than the drain's elevation. In Figure S2.1, water table nodes are labeled blue and the corresponding heads have orange labels. The water tables obtained via the Dupuit assumption are always lower than the simulated water table since the vertical flow and seepage face are not considered. Note that the heads at water table nodes are higher than their elevation, but below the elevation of the nearest dry node above them. The water tables simulated with our method are nearly the same as the MODFLOW simulation. Additionally, we can see the seepage face boundaries on both sides, which evidently do not exist in the analytical solution. The analysis demonstrates the effectiveness of our algorithm.

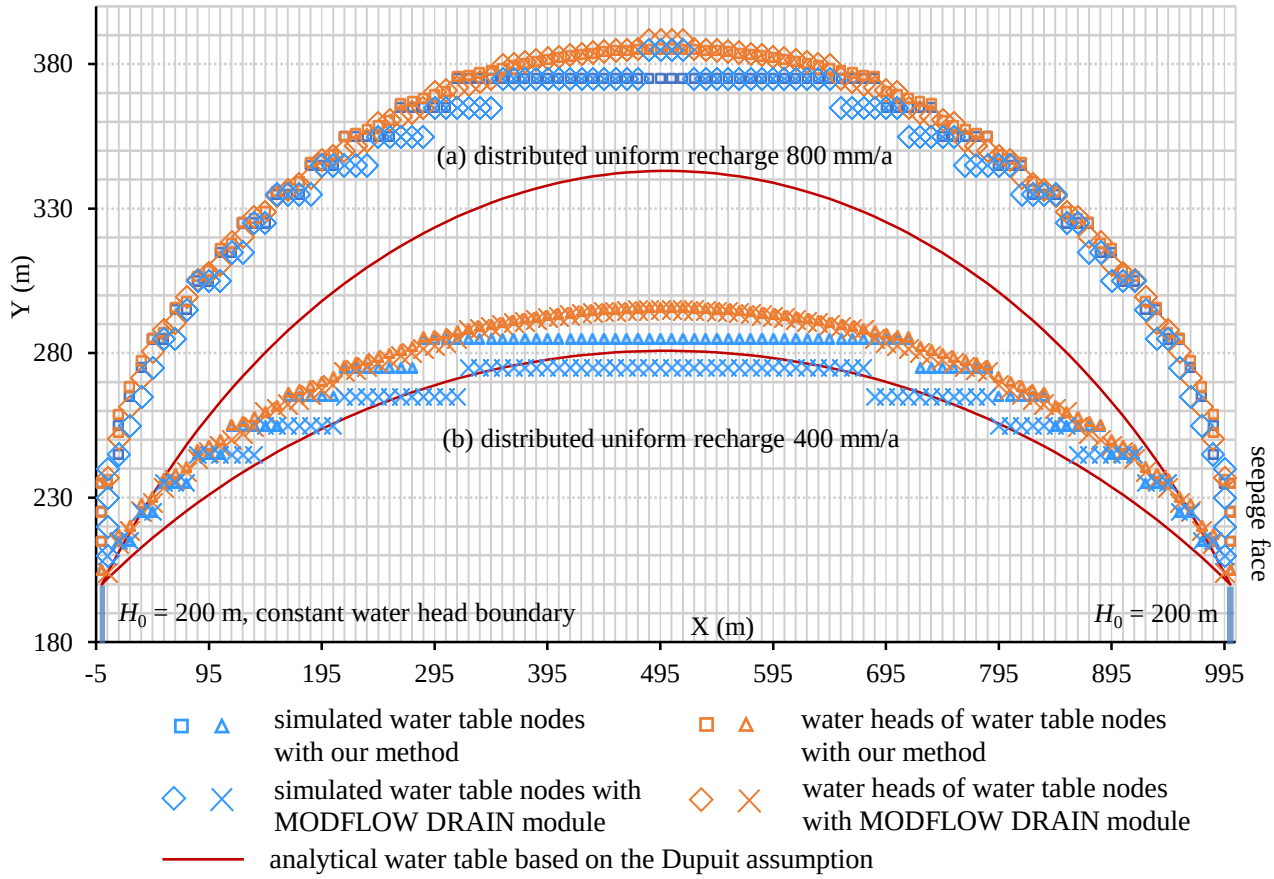

Figure S2.1: Water tables and corresponding heads validation with MODFLOW and Dupuit analytical models for two distributed uniform recharge conditions.

S3 Modeling a water table in a heterogeneous fractured aquifer

The next step is to test the solution for heterogeneous network. We use the same setting as for the homogenous network but with random generation of fractures and two recharge conditions, 200 mm/a and 400 mm/a. The equivalent horizontal and vertical K values are 0.00469 m/d and 0.00434 m/d, respectively. The number of outer iterations in all evolving time steps varied from 5 to 35. The process of searching for a water table takes approximately 3 to 4 hours during the initial modeling stages of karst evolution, and it is performed on a high-performance computing platform that utilizes 8 cores.

The fracture flow and water table data are shown in Figure S3.1 and Figure S3.2. The water table is discontinuous because of the inhomogeneous distribution of fractures. Only a few nodes for the simulated water table are lower than the analytical water table. The difference between the elevation and head at water table nodes varies due to the heterogeneity of the network. The seepage faces above the constant head boundaries on the both sides of the domain, are successfully simulated as the Signorini boundary (Jiang et al., 2013). Considering these two recharge conditions, the algorithm performed well in modelling the water table in heterogeneous network.

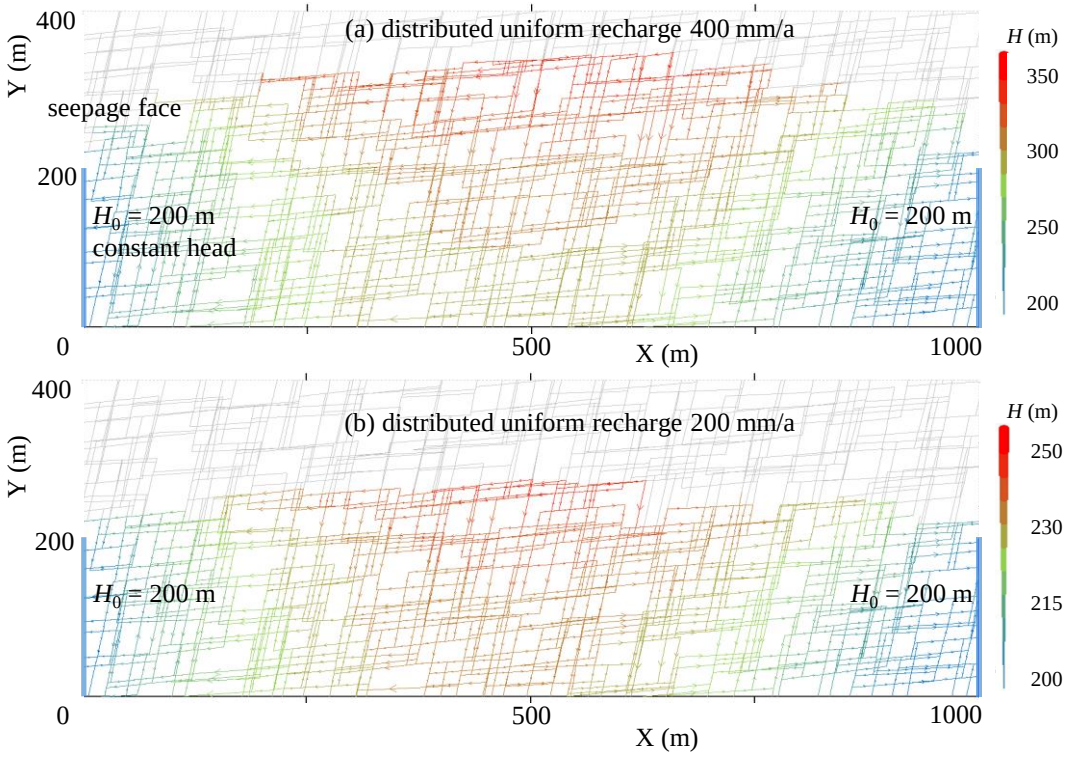

Figure S3.1. Modelling the phreatic flow in random fractures under 400mm/a and 200mm/a distributed uniform recharge conditions.

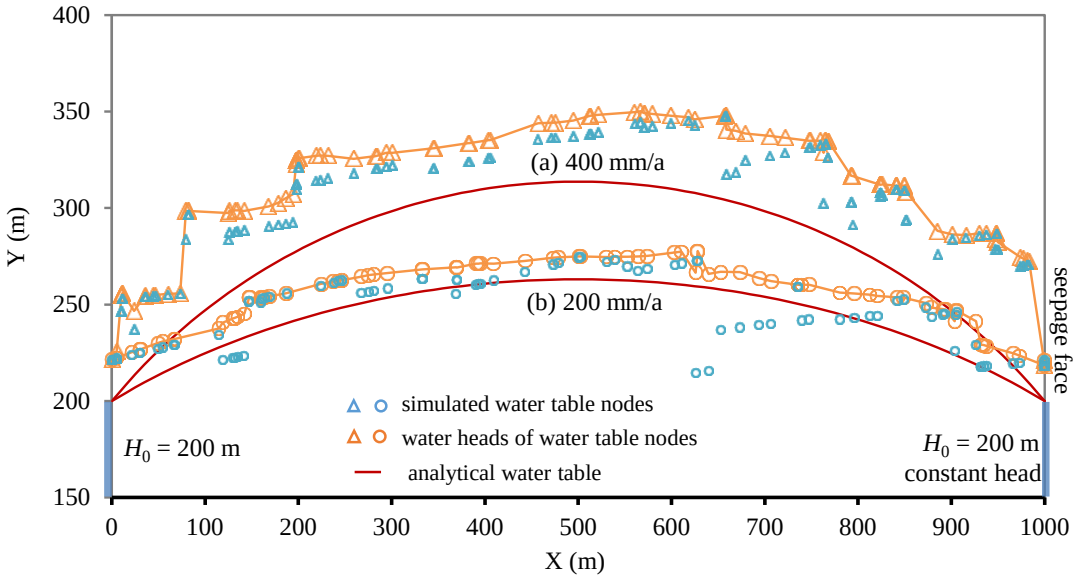

Figure S3.2: The simulated and analytical results of random fracture water tables and water heads of corresponding nodes.

S4 Changes of concentration within individual fracture and on a network scale

S4.1 Dissolution and change of concentration along an individual fracture

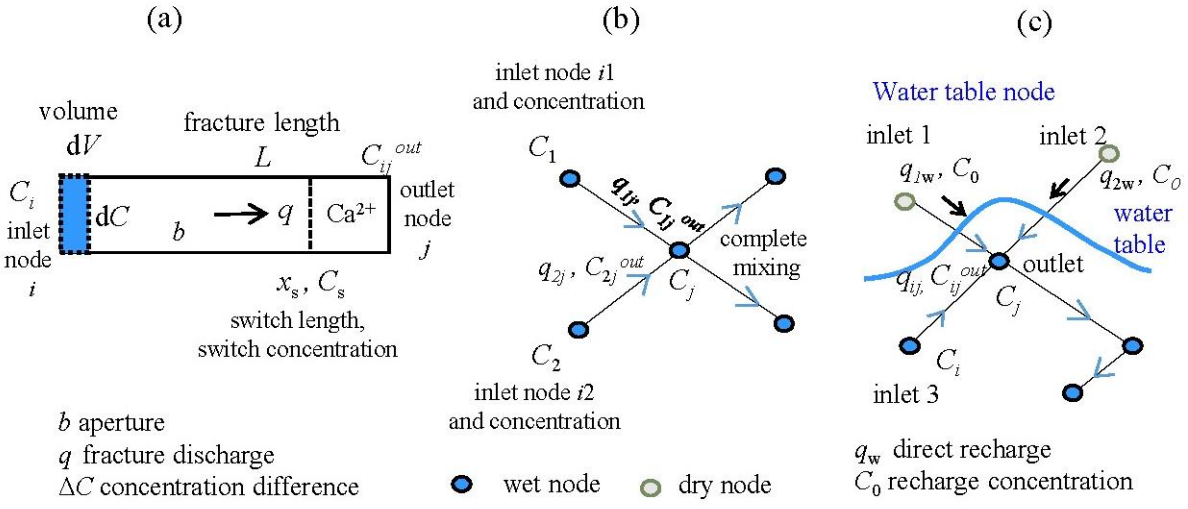

Figure S4.1: Calculating Ca^{2+} concentration along one single fracture and at fractures joint node and near the water table.

To calculate change of concentration within a single fracture, we use a Lagrangian approach and imagine a water parcel with volume $dV=Pdx$ moving along the fracture with velocity $v=Q/A$, where A is a flow crosssection, and calculate the change of concentration within the parcel (Figure S4.1). In a time dt the change of concentration in a parcel is equal to:

$$dC = F(c) \cdot P \cdot dx \cdot \ dt/dV \tag{S2}$$

Where P is flow perimeter and Pdx is the surface area of water/rock contact. Rearranging the equation gives:

$$\int_{C_i}^{c(x)} \frac{dc}{F(c)} = \frac{P}{Q}x = \frac{2(b+w)}{qw}x \approx \frac{2}{q}x \tag{S3}$$

The last term is an approximation for a wide fracture with the lateral width w and aperture b, where $w>>b$; q is flow rate per unit width. Using rate Equations (Eq. 7 and Eq. 8) for $F(c)$, we get:

$$C(x) = C_{\mathrm{eq}} - \ (C_{\mathrm{eq}} - C_i)e^{-\left(\frac{2k_1}{q\,C_{\mathrm{eq}}}x\right)}, \quad (C < C_s\,) \tag{S4}$$

$$C(x) = C_{\mathrm{eq}} - C_{\mathrm{eq}}(C_{\mathrm{eq}} - C_i)\ \sqrt[3]{\frac{q\ C_{\mathrm{eq}}}{(C_{\mathrm{eq}} - C_i)^3 6k_4 x + q\ {C_{\mathrm{eq}}}^4}}, (C_s < C < C_{\mathrm{eq}}) \tag{S5}$$

Where k_1 and k_4 are rate constants. C_{eq} and C_s are the equilibrium concentration and the switch concentration of Ca^{2+} ions.

The change of concentration ΔC at the outlet of the fracture is given by:

$$\Delta C = C_{eq} - C_{eq}e^{-\left(\frac{2k_1}{q\,C_{eq}}L\right)} + C_i\left(e^{-\left(\frac{2k_1}{q\,C_{eq}}L\right)} - 1\right), (\ C_i < C_s, x_s > L) \tag{S6}$$

$$\Delta C = C_{eq} - C_i - 0.1\ C_{eq}^2\ \sqrt[3]{\frac{q\ C_{eq}}{(0.1C_{eq})^3 6k_4 L + q\ {C_{eq}}^4}}, (C_i < C_s, x_s < L) \tag{S7}$$

$$\Delta C = C_{eq} - C_i - C_{eq}^2\ \sqrt[3]{\frac{q\ C_{eq}}{(C_{eq} - C_i)^3 6k_4 L + q\ {C_{eq}}^4}} + C_{eq}C_i\ \sqrt[3]{\frac{q\ C_{eq}}{(C_{eq} - C_i)^3 6k_4 L + q\ {C_{eq}}^4}}, (\ C_i > C_s) \tag{S8}$$

Where x_s is the switch distance of C_s. If $C_i < C_s$ and $x_s > L$, dissolved mass is calculated from Eq. (S6). If $C_i < C_s$ and $x_s < L$, Eq. (S7) is used. If $C_i > C_s$, Eq. (S8) is used for dissolved mass directly.

S4.2 Following concentration at the network scale

To assure that concentrations at the input nodes are always known, we follow the procedure of Siemers and Dreybrodt (1998) and Gabrovšek and Dreybrodt (2000). The process begins at the network's boundary nodes with the highest hydraulic heads, where head or flux values and concentrations are prescribed. Calculations then proceed sequentially along the hydraulic gradient. As illustrated in Figure S4.1(b and c), the concentration C_j at the node j is calculated using the complete mixing assumption. This involves computing the flow-weighted average of the incoming concentrations:

$$c_j = \frac{\sum_i C_{ij}^{out} q_{ij} + \sum_k C_0 q_{wk}}{\sum_i q_{ij} + \sum_k q_{wk}} \quad \text{(S9)}$$

Where q_{wk} and C_0 are flow and concentration of direct recharge at water table nodes; q_{ij} and C_{ij}^{out} are the output flow and concentration of fractures connecting nodes i and j; i sums over confined nodes that deliver flow to j, and k runs over direct input at the water table.

References

Harbaugh, A. W., Banta, E. R., Hill, M. C., and McDonald, M. G.: MODFLOW-2000, the US Geological Survey modular ground-water model: User guide to modularization concepts and the ground-water flow process, U.S. GEOLOGICAL SURVEY, Open-File Report 00-92, https://doi.org/10.3133/ofr200092, 2000.

Jiang, Q., Yao, C., Ye, Z., and Zhou, C.: Seepage flow with free surface in fracture networks, Water Resour. Res., 49, 176-186, https://doi.org/10.1029/2012WR011991, 2013.